Title
PRODUCT MASS AND CHARGE DISTRIBUTIONS IN THE REACTION OF 48Ca WITH SILVER

Author
Loveland, W.

Publication Date
1977-06-01

Submitted to Nuclear Physics A

PRODUCT MASS AND CHARGE DISTRIBUTIONS IN THE REACTION OF ^{48}Ca WITH SILVER

W. Loveland, D. J. Morrissey, R. J. Otto, and
G. T. Seaborg

June 1977

Prepared for the U. S. Energy Research and
Development Administration under Contract W-7405-ENG-48

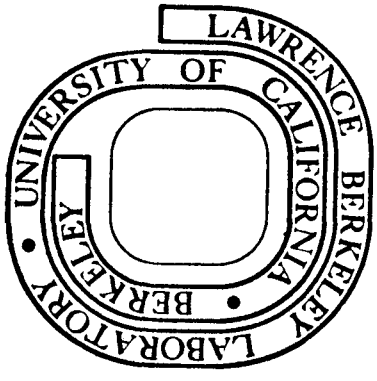

DISCLAIMER

PRODUCT MASS AND CHARGE DISTRIBUTIONS IN THE REACTION OF ^{48}Ca WITH SILVER[†]

W. Loveland,[††] D. J. Morrissey, R. J. Otto and G. T. Seaborg

Lawrence Berkeley Laboratory
and Department of Chemistry
University of California
Berkeley, California 94720

June 1977

ABSTRACT

Product mass and charge distributions have been measured radiochemically for the reaction of natural Ag with ~224 MeV ^{48}Ca ions. Evaporation residue (σ_{ER}) and fission cross sections (σ_F) of 700 ± 100 mb and 100±50 mb, respectively, were deduced from an analysis of the mass distribution. Comparison of these data with results of similar studies of the ^{40}Ar + ^{109}Ag reaction show that the complete fusion cross sections in these reactions can be understood in terms of the critical distance concept. However, the ratio of σ_F/σ_{ER} is lower than expected based on calculations using the ALICE Code for the ^{48}Ca induced reaction.

NUCLEAR REACTIONS ^{107,109}Ag(^{48}Ca,X), for $11 \leq Z_X \leq 66$, $24 \leq A_X \leq 152$
$E_{lab} \approx 224$ MeV; measured $\sigma(A, Z_{product})$

[†]Work supported in part by the Division of Physical Research of the U.S. Energy Research and Development Administration.

[††]Permanent address: Department of Chemistry, Oregon State University, Corvallis, Oregon 97331.

1. Introduction

The reaction of ^{48}Ca ions with very heavy neutron-rich targets is thought to be one of the most promising ways to synthesize superheavy elements (SHE) in the laboratory.[1] Recently, an extensive research effort to synthesize SHE's with ^{48}Ca induced reactions has been made at Berkeley[2] and Dubna[3] with preliminary results indicating that the upper limit for the cross section for the formation of SHE's with half-lives in the range from days to years in the reaction of 255 MeV ^{48}Ca with ^{248}Cm is $\lesssim 10^{-35}$ cm^2. To help understand these negative results and because of the general interest in studying nuclear reactions involving a doubly magic, neutron-rich projectile, we undertook a systematic study of the reaction of ^{48}Ca with a wide range of medium and heavy mass targets, focusing upon the complete fusion process. In this paper, we report some of the first results of this general study, i.e., the product mass and charge distributions for the reaction of ~224 MeV ^{48}Ca with natural Ag.

Silver was chosen as the target for these studies of the complete fusion process in the reaction of ^{48}Ca with medium mass targets in hopes of comparing our results with the well-characterized ^{40}Ar + ^{109}Ag reaction. Galin *et al.*[4] have studied deep-inelastic scattering in the Ag + ^{40}Ar reaction while Britt *et al.*[5] have made extensive studies of evaporation residues and fission in this reaction. Hille *et al.*[6] measured a number of individual radionuclide production

cross sections for the $^{40}Ar + ^{109}Ag$ reaction. It was thought to be of interest to compare our measurements for the reaction of doubly magic ^{48}Ca + Ag with those for the ^{40}Ar + Ag reaction in view of predictions[7] of smaller complete fusion cross sections in the ^{48}Ca reaction. Another interesting comparison between ^{40}Ar + Ag and ^{48}Ca + Ag reactions turned out to be the relative magnitudes of the fission and evaporation residue cross sections.

In Section 2 of this paper, we describe the experimental procedures used in this work while we present our product mass and charge distributions along with the deduction of complete fusion, evaporation residue and fission cross sections in Section 3. Section 4 of this paper is devoted to a discussion of the systematics of complete fusion cross sections for ^{40}Ar induced reactions and how our ^{48}Ca data fit into a theoretical description of these reactions in terms of a "critical distance" approach[7] to understanding these reactions. Also, the ratios of evaporation residue to fission cross sections are compared with the predictions of statistical models for the de-excitation of highly excited, high angular momentum nuclei.

2. Experimental Procedure

A natural Ag foil of thickness 230 mg/cm^2 was irradiated by a ^{48}Ca beam of average intensity 5.4×10^{13} particles/min for ~450 min at the SuperHILAC. The ^{48}Ca projectile energy as it entered the foil was 303 MeV and was periodically monitored throughout the irradiation by

measuring the energy of ^{48}Ca ions elastically scattered from a thin Au foil placed in front of the Ag target. The effective ^{48}Ca energy in the thick target (see Section 3) was calculated to be $E_{lab} \simeq 224$ MeV. The Ag target for this experiment acted as a collimator for other experiments performed at the same time involving ^{208}Pb[8] and ^{248}Cm[2] targets and thus had a 6.35 mm hole drilled through the center of it. Due to difficulties in absolute monitoring of the number of ions striking the Ag collimator target, all yields measured in this work were relative yields which were then converted to absolute cross sections based upon comparison of the experimental mean total reaction cross section with the mean geometric reaction cross section (see Section 3). While a separate irradiation to study the ^{48}Ca + Ag reaction would have been preferable, the extremely high cost and low availability of the ^{48}Ca beam prohibited such experiments.

Following irradiation, the target was divided into two fractions. The Sc reaction products were chemically separated from the first fraction by solvent extraction[9] and a Sc sample prepared for γ-ray spectrometry. The γ-radiation from the separated Sc sample and the second fraction of the Ag target was then measured with a 54 cc Ge(Li) spectrometer system that has a system resolution of 2.1 keV at the 1332 keV line of ^{60}Co. Gamma ray spectra were measured starting one hour after irradiation and continuing for a period of one month. The samples were

counted in a fixed geometry and an NBS-calibrated mixed γ-ray source (SRM-4216C) was used for determination of the energy and efficiency calibration of the spectrometer.

Absolute intensities for each γ-ray observed in each spectrum were then extracted from the data using the peak-fitting program SAMPO.[10] Decay curves were constructed for each γ-ray line and a tentative assignment of the line to specific radionuclide(s) was made using the interactive graphics program TAU2.[11] This program[+], the key to our γ-spectrometric method of measuring reaction product mass distributions, allows one to select from a very current compilation of nuclear data[12] a radionuclide (or combination of radionuclides), with an appropriate γ-ray energy and half-life, as a possible assignment to each γ-ray observed. The program then performs the best least squares fitting of the decay curves with the assumed radionuclide decay properties, accounts for growth and decay and multicomponent decay curves, and yields the number of atoms of each identified radionuclide at the end of bombardment. Gamma rays with energies less than ~90 keV or greater than 2 MeV are generally not treated in this analysis. The data are reviewed at this point to make sure that all γ-rays assigned to a specific radionuclide have the right intensity ratio[12] and that all γ-rays in the decay scheme of interest with intensities equal to or greater than the lowest observed intensity are also seen. If this intensity criterion is not met, the identification is rejected unless it can be shown

---

[+]Available upon request to the authors.

that more intense γ-rays from another radionuclide have masked the line(s) of interest. Typically 1/3 of the radionuclide assignments made by the TAU2 program are rejected at this point. When several γ-rays of the same nuclide are observed, the number of atoms of that radionuclide is calculated from the weighted average of all the corrected γ-ray intensities.

An iterative process using the programs CROSS[+] and MASSY[+] was then used to deduce independent yield cross sections from the measured number of atoms of each radionuclide at end of bombardment.[++] A Gaussian distribution of the yields of various isobars of the form

$$P(Z) = \frac{1}{(2\pi\sigma^2)^{1/2}} \exp\left[\frac{(Z-Zp)^2}{2\sigma^2}\right]$$

was assumed for each A with arbitrary values of the parameters, Zp, the most probable product charge and σ, the Gaussian width parameter, being chosen. Corrections were then made based upon these Gaussian yield curves for any grandparent-parent-daughter decay during or after the bombardment, resulting in a pseudo independent yield cross section for each radionuclide that represented an isobaric cumulative yield. These pseudo-cross sections were then compared with the assumed Gaussian primary product distribution, the parameters of the

---

[+]Available upon request from authors.

[++]An effective target thickness of ~14 mg Ag/cm^2 was assumed, corresponding to a reaction barrier[13] (center of mass) of 110 MeV.

Gaussian distribution adjusted to fit the data, and the process iterated until convergence was achieved.

3. Results

The independent yield radionuclide cross sections for the ^{48}Ca + Ag reaction derived from the above procedures are shown in Figure 1(a) and tabulated in Table 1. The apparent scatter in the data in Figure 1(a) occurs because the independent yields generally represent only a fraction of the total mass yield. The (Z,A) distributions of the products for various mass regions are shown in Figure 1(b). The Gaussian charge distribution curves fitted to the data of Figures 1(a) and (b) were integrated to give the yield of each A where a radionuclide was observed in the reaction. The resulting product post-neutron emission mass distribution is shown in Figure 1(c) along with the data of Hille et al.[6] In preparing Figure 1(c), the data were normalized so that the experimental total reaction cross section (the area under the curve in Figure 1(c)) equals the mean geometric reaction cross section for a thick target reaction as given by:

$$\bar{\sigma}_R = \frac{\pi R^2 \int_B^E (1-(\frac{B}{E}))dE}{E-B} = 1319 \text{ mb} \qquad (1)$$

where the interaction radius R=12.1 fm, the interaction barrier B=110 MeV, and the incident projectile energy (cms) E=209.8 MeV. This would imply the effective projectile energy in the thick target in the center of mass system was

$$E_{eff} = \frac{B}{1-\frac{\bar{\sigma}_R}{\pi R^2}} = 155 \text{ MeV} \qquad (2)$$

i.e., $E_{eff}(lab) \simeq 224$ MeV.

The evaporation residue cross section, σ_{ER}, was taken to be the area under the curve for $124 \leqslant A \leqslant 153$ and is 700±100 mb. To extract the fission cross section, σ_F, we did a least squares decomposition of the mass yield curve for $24 \leqslant A \leqslant 124$ into components representing deep inelastic scattering, fission and quasi-elastic scattering. Based upon an extrapolation of the data of Britt et al.,[5] we chose Gaussian shapes of specific width and center for the mass distribution associated with each of these components. The fission mass distribution was assumed to have a FWHM of 28 A units centered at A=71.5. The deep inelastic distribution was represented by two Gaussian distributions (constrained to have equal area) of FWHM 27 and 40 A units, centered at A=44 and A=104, respectively. The quasi-elastic distribution was also represented by two Gaussian distributions of equal area, centered at A=48 and 108 of FWHM ~4 A units. The magnitude of each component of the mass distribution was then determined by a non-linear least squares fit of the component shapes to the data. The results give $\sigma_F \simeq 100 \pm 10$ mb, $\sigma_{QUASIELASTIC} \simeq 250 \pm 25$ mb and $\sigma_{DEEP\ INELASTIC} \simeq 270 \pm 30$ mb. The above estimate of uncertainty in the fission cross section does not take into account uncertainties in the shapes of the deep inelastic component[†] and should probably

---

[†]The measured angle-integrated Z distributions for deep inelastic scattering for ^{40}Ar + Ag of ref. 4 and 5 differ. Based upon our experience with other mass distributions and their deep inelastic components,[8,11,14] and the data of other workers,[15] we have used the data of reference 5 to represent the deep inelastic component of the mass distribution.

be regarded as $\sigma_F \sim 100 \pm 50$ mb, taking these uncertainties into account. From these cross sections, we calculate the complete fusion cross section, σ_{CF} $(=\sigma_{ER} + \sigma_F)$, as 800±110 mb.

4. Discussion of Results

Glas and Mosel[7] have shown that the cross section for complete fusion as predicted by the critical distance formulation is given by:

$$\sigma_{CF} = \left(\frac{\hbar\omega\vartheta_B}{2\mu E}\right) \ell n \left\{ \frac{1 + \exp[2\pi(E-V_B)/\hbar\omega]}{1 + \exp[2\pi(E-V_B-\vartheta_{cr}(E-V_{cr})/\vartheta_B)\hbar\omega]} \right\} \quad (3)$$

where ϑ_B, V_B are the moment of inertia and potential energy at the interaction barrier (radius R_B) while ϑ_{cr}, V_{cr} are the same quantities at the critical distance R_{cr}. E is the projectile cms energy and $\hbar\omega$ is the barrier curvature. Based upon an analysis of a large amount of experimental data, Lefort[16] and co-workers have found that

$$R_{cr} = (1.0 \pm 0.07)\ (A_1^{1/3} + A_2^{1/3})\ \text{fm} \quad (4)$$

Similarly Ngo[17] has shown that for $Z_1\ Z_2 < 1000$

$$V_{cr} = (0.124275\ Z_1\ Z_2 - 17.6)\ \text{MeV} \quad (5)$$

Using equations 3, 4, 5 and the relation $R_B = 1.44\ (A_1^{1/3} + A_2^{1/3})$ fm, a value of $\hbar\omega$ of 5 MeV, one calculates σ_{CF} for the ^{48}Ca + Ag reaction to be 797 mb, a value in remarkably good agreement with the experimental value of 800±110 mb.

Since equations 4 and 5 represent a systemization of a large amount of data, one must conclude that the prediction of Glas and Mosel[7] that one should find a smaller value of R_{cr} than usually seen in heavy ion reactions when one reaction partner is doubly magic is not verified. It may be that at the bombarding energies involved in this work (E-B ≃45 MeV) nuclear shell effects are not important in determining the reaction dynamics or the effect of only one doubly magic reaction component (ie, the projectile but not the target) is not sufficient to affect the experimental value of σ_{CF}.

Another intriguing feature of the data is the ratio σ_F/σ_{ER} which is $\frac{100\pm 50}{700\pm100}$ for this study and was found to be $\frac{300\pm100}{620\pm 90}$ for the $^{40}Ar + ^{109}Ag$ reaction at E_{cms}=144 MeV by Britt et al.[5] A standard statistical deexcitation calculation involving neutron-fission-charged particle emission competition using the OVERLAID ALICE code[18] with level density parameter ratio a_f/a_n= 1.0, ΔJ=no option and the rotating liquid drop fission barriers of this code, that sums all partial waves up to an $\ell_{cr}=75\hbar$[†], predicts $\frac{\sigma_F}{\sigma_{ER}} = \frac{220}{619}$ for the $^{40}Ar + ^{109}Ag$ reaction, in rough agreement with the experimental data. Using the same parameters to describe the ^{48}Ca + Ag reaction, one calculates that $\frac{\sigma_F}{\sigma_{ER}} \simeq \frac{297}{488}$ when one sums all partial waves up to $\ell_{cr}=79\hbar$.[†] Calculations

---

[†] ℓ_{cr} was calculated from the relation $\ell_{cr}(\ell_{cr}+1) = \frac{2\vartheta_{cr}}{\hbar^2}(E-V_{cr})$ with the previously described values of E, ϑ_{cr}, V_{cr}.

performed with the best new values[19] of the ground state fission barriers give essentially similar results, i.e., an inability to account for the increased survival of the compound nuclei made in the ^{48}Ca + Ag reaction (in both cases, the excitation energies, E~90 MeV, are similar). Since in both cases the rotational energies of the system are quite high for those partial waves contributing most to the complete fusion cross section, the exact ratio of σ_F/σ_{ER} will depend sensitively upon how the fission barrier is lowered as a function of angular momentum. These data may suggest that the prescription of Cohen, Plasil and Swiatecki[20] used in the deexcitation calculation simply are not accurate enough to account for the detailed variation of σ_F/σ_{ER} in the region where the rotating liquid drop fission barriers are small (<2 MeV, as compared to a J=0 barrier of ~30 MeV).

One of us (WDL) wishes to acknowledge gratefully sabbatical leave support from Oregon State University. We are very happy to acknowledge also the assistance of Mrs. Diana Lee in computer processing of the data and for her general role in developing and maintaining the computer programs used in this work.

References

1. W. J. Swiatecki and C. F. Tsang, Lawrence Berkeley Laboratory Report LBL-666, (1972), p. 138.
2. E. K. Hulet et al., Phys. Rev. Lett. (submitted for publication)
3. G. N. Flerov et al., Nucl. Phys. A267 (1976) 359.
4. J. Galin, L. G. Moretto, R. Babinet, R. Schmitt, R. Jared and S. G. Thompson, Nucl. Phys. A255 (1975) 472.
5. H. C. Britt, B. H. Erkkila, R. H. Stokes, H. H. Gutbrod, F. Plasil, R. L. Ferguson and M. Blann, Phys. Rev. C13 (1976) 1483.
6. M. Hille, P. Hille, H. H. Gutbrod and M. Blann, Nucl. Phys. A252 (1975) 496.
7. D. Glas and U. Mosel, Nucl. Phys. A237 (1973) 429.
8. D. J. Morrissey, W. Loveland, R. J. Otto and G. T. Seaborg, Phys. Rev. Lett. (submitted for publication)
9. R. Batzel as described in W. W. Meinke, Univ. of California Radiation Laboratory Report UCRL-432 (1949).
10. J. T. Routti and S. G. Prussin, Nucl, Instr. Meth. 72 (1969) 125.
11. I. Binder, Ph.D. thesis, Lawrence Berkeley Laboratory Report No. LBL-6526, Univ. of California, Berkeley, 1977; I. Binder, M. Di Casa, J. V. Kratz, J. O. Liljenzin and A. E. Norris, Lawrence Berkeley Laboratory Report LBL-2366 (1973) 451.
12. I. Binder, R. Kraus, D. Lee and M. M. Fowler, Lawrence Berkeley Laboratory Report LBL-6515, (1977)

13. L. C. Northcliffe and R. I. Schilling, Nucl. Data A7, 233 (1970).

14. J. V. Kratz, J. O. Liljenzin, A. E. Norris and G. T. Seaborg, Phys. Rev. C12 (1976) 2347.

15. J. R. Huizenga, Comments on Nuclear and Particle Physics VII (1976) 17.

16. M. Lefort, J. de Phys. C5 (1976) 57.

17. C. Ngo, Thesis, Université, Paris-Sud (1975).

18. M. Blann, USERDA Report COO-3494-29 (1976).

19. W. D. Myers and W. J. Swiatecki (private communication).

20. S. Cohen, F. Plasil and W. J. Swiatecki, Ann. Phys. NY (1974) 557.

Table 1

Individual Radionuclide Yields from ~224 MeV ^{48}Ca + Ag

Nuclide	E_γ(keV) of γ-Ray(s) Used to Identify Nuclide	Measured Independent or Partial Cumulative Yield	Calculated Independent Yield (mb)	Mass Yield (mb)
^{24}Na	1368.5	0.128 ± 0.012	0.104 ± 0.010	0.255 ± 0.026
^{28}Mg	1342.2	0.143 ± 0.033	0.133 ± 0.031	0.264 ± 0.062
	1589.4			
^{42}K	1524.7	2.51 ± 0.27	2.51 ± 0.27	11.1 ± 1.2
^{43}K	372.0	3.62 ± 0.43	3.10 ± 0.37	7.7 ± 0.9
	593.5			
^{44}Sc	1157.0	0.124 ± 0.039	0.124 ± 0.039	7.7 ± 3.9
^{44m}Sc	1157.0	0.31 ± 0.33	0.31 ± 0.033	
^{46}Sc	889.3	4.72 ± 0.51	4.72 ± 0.51	57.0 ± 6.2
	1120.5			
^{47}Sc	159.4	10.8 ± 1.0	9.8 ± 1.0	58.5 ± 6.0
^{47}Ca	489.2	39.5 ± 3.4	39.5 ± 3.4	57.5 ± 4.9
	807.9			
^{48}Sc	983.5	10.3 ± 1.8	10.3 ± 1.8	22.7 ± 3.9
	1037.6			
	1212.6			
	1312.1			
^{56}Mn	846.6	3.59 ± 0.86	2.51 ± 0.25	10.9 ± 0.1
^{59}Fe	1099.2	2.92 ± 0.21	2.92 ± 0.21	3.1 ± 0.2
	1291.0			
^{67}Ca	184.5	2.50 ± 0.21	2.50 ± 0.21	12.0 ± 1.0
^{69}Ge	1106.4	1.24 ± 0.14	1.24 ± 0.14	9.2 ± 1.0
^{69m}Zn	438.7	2.10 ± 0.17	2.09 ± 0.17	7.8 ± 0.6
^{71}As	174.9	1.55 ± 0.10	1.55 ± 0.10	17.1 ± 1.1
^{72}Ga	629.9	1.42 ± 0.10	1.41 ± 0.10	9.9 ± 0.7
	1861.1			
^{72}As	834.0	3.60 ± 0.59	3.58 ± 0.59	13.8 ± 2.3

Table 1

Individual Radionuclide Yields from ~224 MeV ^{48}Ca + Ag

Nuclide	E_γ(keV) of γ-Ray(s) Used to Identify Nuclide	Measured Independent or Partial Cumulative Yield	Calculated Independent Yield (mb)	Mass Yield (mb)
^{73}Se	360.9	0.25 ± 0.039	0.25 ± 0.039	4.2 ± 0.7
^{74}As	595.9	5.18 ± 0.34	5.18 ± 0.34	8.7 ± 0.6
^{75}Se	136.0	2.17 ± 0.21	2.15 ± 0.21	5.2 ± 0.5
^{76}As	559.5	8.35 ± 0.68	8.35 ± 0.68	31.2 ± 2.5
^{77}Br	238.9	1.99 ± 0.21	1.97 ± 0.21	5.9 ± 0.6
	249.7			
	385.1			
	520.7			
	579.4			
^{80m}Br	665.6	5.50 ± 1.93	5.50 ± 1.93	13.1 ± 4.6
^{82}Br	554.3	2.68 ± 0.70	2.68 ± 0.70	43.7 ± 11.4
	619.1			
	698.4			
	827.8			
	1007.6			
	1317.4			
	1474.8			
^{82m}Rb	554.3	2.32 ± 0.21	2.32 ± 0.21	5.6 ± 0.5
	698.4			
	827.6			
	1007.6			
	1317.5			
^{84}Rb	881.5	3.96 ± 0.37	3.96 ± 0.37	7.3 ± 0.7
^{86}Y	627.7	1.33 ± 0.35	1.31 ± 0.35	5.0 ± 1.3
	644.8			
	1076.8			
	1153.0			
	1253.1			

Table 1

Individual Radionuclide Yields from ~224 MeV ^{48}Ca + Ag

Nuclide	E_γ(keV) of γ-Ray(s) Used to Identify Nuclide	Measured Independent or Partial Cumulative Yield	Calculated Independent Yield (mb)	Mass Yield (mb)
	1349.2			
	1854.4			
	1920.7			
^{87}Y	388.4	4.49 ± 0.46	4.42 ± 0.45	9.1 ± 0.9
	484.8			
^{89}Zr	909.2	2.81 ± 0.28	2.78 ± 0.28	6.7 ± 0.7
^{90m}Y	202.4	1.95 ± 0.17	1.95 ± 0.17	7.3 ± 0.6
^{93m}Mo	684.6	1.07 ± 0.11	1.07 ± 0.11	4.1 ± 0.4
	1477.2			
^{94}Tc	849.7	0.37 ± 0.34	0.37 ± 0.34	6.1 ± 0.6
	870.9			
^{96}Nb	460.0	0.83 ± 0.12	0.83 ± 0.12	13.7 ± 1.9
	568.9			
	1091.3			
	1497.7			
^{96}Tc	778.2	1.83 ± 0.20	1.83 ± 0.20	4.4 ± 0.5
	812.5			
	849.9			
^{97}Ru	215.7	0.70 ± 0.17	0.70 ± 0.17	5.1 ± 1.2
	324.5			
^{99}Mo	140.5	0.36 ± 0.035	0.36 ± 0.035	16.9 ± 1.7
^{100}Ru	539.6	0.85 ± 0.12	0.84 ± 0.12	7.0 ± 1.0
	822.5			
	1362.1			
	1553.4			
^{101m}Rh	306.8	1.97 ± 0.21	1.97 ± 0.21	7.3 ± 0.8
^{105}Ru	724.2	0.15 ± 0.02	0.15 ± 0.02	5.6 ± 0.6

Table 1

Individual Radionuclide Yields from ~224 MeV ^{48}Ca + Ag

Nuclide	E_γ(keV) of γ-Ray(s) Used to Identify Nuclide	Measured Independent or Partial Cumulative Yield	Calculated Independent Yield (mb)	Mass Yield (mb)
^{106m}Ag	221.5 328.3 406.0 429.5 450.8 703.3 717.1 792.8 803.9 824.5 1045.7 1127.8 1199.1 1222.8 1527.0 1572.1	4.13 ± 0.18	4.13 ± 0.18	12.5 ± 0.5
^{106m}Rh	406.0 429.4 450.8 717.2 804.6 1127.7 1529.4	1.90 ± 0.29	1.90 ± 0.29	14.6 ± 2.2
^{110m}In	707.4 884.7 937.5	0.64 ± 0.23	0.64 ± 0.23	3.01 ± 1.1
^{111}In	171.3 245.4	2.28 ± 0.23	2.24 ± 0.23	5.7 ± 0.6

Table 1

Individual Radionuclide Yields from ~224 MeV ^{48}Ca + Ag

Nuclide	E_γ(keV) of γ-Ray(s) Used to Identify Nuclide	Measured Independent or Partial Cumulative Yield	Calculated Independent Yield (mb)	Mass Yield (mb)
^{118m}Sb	1050.7 1229.6	0.28 ± 0.045	0.28 ± 0.045	0.61 ± 0.10
^{139}Xe	564.0	0.0573 ± 0.006	0.0573 ± 0.006	0.19 ± 0.02
^{139}Ce	165.8	0.0405 ± 0.105	0.0173 ± 0.00447	4.3 ± 1.1
^{145}Eu	542.6 653.5 893.7 1658.7 1804.4 1876.8	22.4 ± 2.6	22.3 ± 2.6	54.9 ± 6.3
^{147}Gd	229.9 310.5 370.5 396.1 610.8 625.2 754.9 765.5 861.5 928.0 995.0 1068.0 1130.0 1325.3 1325.0 1794.2	34.0 ± 3.1	34.0 ± 3.1	110.4 ± 10.1
^{147}Eu	798.8	24.2 ± 1.2	22.7 ± 1.1	36.6 ± 1.8

Table 1

Individual Radionuclide Yields from ~224 MeV ^{48}Ca + Ag

Nuclide	E_γ(keV) of γ-Ray(s) Used to Identify Nuclide	Measured Independent or Partial Cumulative Yield	Calculated Independent Yield (mb)	Mass Yield (mb)
	933.1			
	955.9			
	1256.0			
^{149}Gd	149.6	21.9 ± 0.8	21.0 ± 0.8	31.3 ± 1.2
	272.0			
	346.5			
	534.2			
	645.2			
	788.6			
^{150}Tb	638.0	7.35 ± 0.87	7.30 ± 0.86	14.4 ± 1.7
	792.3			
	880.3			
	1045.4			
^{151}Tb	108.1	33.5 ± 8.4	32.6 ± 8.2	47.9 ± 12.0
	180.1			
	251.8			
	287.2			
	380.1			
	427.0			
	443.8			
	479.2			
	605.5			
	731.8			
^{152}Tb	271.1	32.6 ± 3.8	29.4 ± 3.4	54.3 ± 6.4
	411.1			
	586.3			
	675.3			
	703.0			

Table 1

Individual Radionuclide Yields from ~224 MeV ^{48}Ca + Ag

Nuclide	E_γ(keV) of γ-Ray(s) Used to Identify Nuclide	Measured Independent or Partial Cumulative Yield	Calculated Independent Yield (mb)	Mass Yield (mb)
	970.4			
	1109.2			
	1137.6			
	1261.4			
	1411.5			
	1517.8			
	1902.4			
	1941.1			
^{152}Dy	256.8	14.6 ± 1.4	14.5 ± 1.4	35.6 ± 3.6
^{153}Tb	102.3	4.68 ± 2.52	2.79 ± 1.50	11.2 ± 6.0
	109.7			
	129.2			

Figure Captions

Fig. 1 (a) Independent yield formation cross sections for individual radionuclides.

Fig. 1 (b) Contour lines of equal independent yields in millibarns.

Fig. 1 (c) Total integrated mass yields. The dashed curve is intended as a guide to the data. The solid curve is for the reaction $^{40}Ar + ^{109}Ag$ (ref. 6).

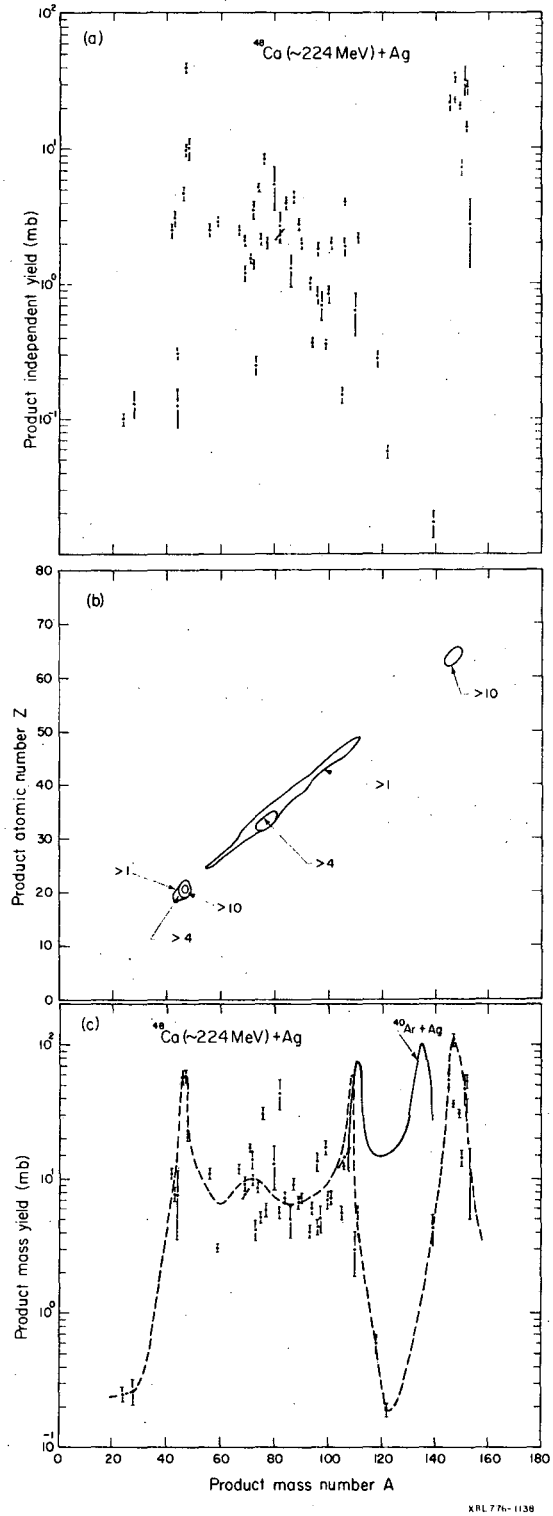
(a)
^{48}Ca (~224 MeV) + Ag
Product independent yield (mb)
(b)
>10
>1
>4
>1
>10
>4
Product atomic number Z
(c)
^{48}Ca (~224 MeV) + Ag
^{40}Ar + Ag
Product mass yield (mb)
Product mass number A
XBL 776-1138

Fig. 1 a, b, and c

TECHNICAL INFORMATION DIVISION
LAWRENCE BERKELEY LABORATORY
UNIVERSITY OF CALIFORNIA
BERKELEY, CALIFORNIA 94720